OPEN ACCESS

Original research

Lactobacillus gallinarum-derived metabolites boost anti-PD1 efficacy in colorectal cancer by inhibiting regulatory T cells through modulating IDO1/Kyn/AHR axis

Winnie Fong,[1] Qing Li,[1,2] Fenfen Ji,[1] Wei Liang,[3] Harry Cheuk Hay Lau ,[1] Xing Kang,[1] Weixin Liu,[1] Kenneth Kin-Wah To,[4] Zhong Zuo,[4] Xiaoxing Li ,[3] Xiang Zhang,[1] Joseph JY Sung ,[5] Jun Yu [1]

► Additional supplemental material is published online only. To view, please visit the journal online (http://dx.doi.org/10.1136/gutjnl-2023-329543).

For numbered affiliations see end of article.

Correspondence to
Professor Jun Yu, Institute of Digestive Disease, Department of Medicine and Therapeutics, Prince of Wales Hospital, The Chinese University of Hong Kong, Hong Kong, China; junyu@cuhk.edu.hk

Received 19 January 2023
Accepted 16 August 2023
Published Online First 28 September 2023

To cite: Fong W, Li Q, Ji F, *et al*. *Gut* 2023;**72**:2272–2285.

ABSTRACT

Objective Gut microbiota is a key player in dictating immunotherapy response. We aimed to explore the immunomodulatory effect of probiotic *Lactobacillus gallinarum* and its role in improving anti-programmed cell death protein 1 (PD1) efficacy against colorectal cancer (CRC).

Design The effects of *L. gallinarum* in anti-PD1 response were assessed in syngeneic mouse models and azoxymethane/dextran sulfate sodium-induced CRC model. The change of immune landscape was identified by multicolour flow cytometry and validated by immunohistochemistry staining and in vitro functional assays. Liquid chromatography-mass spectrometry was performed to identify the functional metabolites.

Results *L. gallinarum* significantly improved anti-PD1 efficacy in two syngeneic mouse models with different microsatellite instability (MSI) statuses (MSI-high for MC38, MSI-low for CT26). Such effect was confirmed in CRC tumourigenesis model. *L. gallinarum* synergised with anti-PD1 therapy by reducing $Foxp3^+$ $CD25^+$ regulatory T cell (Treg) intratumoural infiltration, and enhancing effector function of $CD8^+$ T cells. *L. gallinarum*-derived indole-3-carboxylic acid (ICA) was identified as the functional metabolite. Mechanistically, ICA inhibited indoleamine 2,3-dioxygenase (IDO1) expression, therefore suppressing kynurenine (Kyn) production in tumours. ICA also competed with Kyn for binding site on aryl hydrocarbon receptor (AHR) and antagonised Kyn binding on $CD4^+$ T cells, thereby inhibiting Treg differentiation in vitro. ICA phenocopied *L. gallinarum* effect and significantly improved anti-PD1 efficacy in vivo, which could be reversed by Kyn supplementation.

Conclusion *L. gallinarum*-derived ICA improved anti-PD1 efficacy in CRC through suppressing CD4+Treg differentiation and enhancing CD8+T cell function by modulating the IDO1/Kyn/AHR axis. *L. gallinarum* is a potential adjuvant to augment anti-PD1 efficacy against CRC.

WHAT IS ALREADY KNOWN ON THIS TOPIC

⇒ The gut microbiota is emerging as an important factor dictating immune checkpoint blockade response in human cancers.

WHAT THIS STUDY ADDS

⇒ *Lactobacillus gallinarum* improved anti-PD1 efficacy in both MSI-high and MSI-low colorectal cancer (CRC) tumours by suppressing intratumoural infiltration of regulatory T cells (Tregs).

⇒ *L. gallinarum*-derived indole-3-carboxylic acid (ICA) modulated antitumour immunity by inhibiting IDO1 expression in tumours and lowered kynurenine production in the tumour microenvironment.

⇒ *L. gallinarum*-derived ICA antagonised kynurenine-induced aryl hydrocarbon receptor activation and inhibited subsequent Treg differentiation.

HOW THIS STUDY MIGHT AFFECT RESEARCH, PRACTICE OR POLICY

⇒ *L. gallinarum* may be leveraged as a novel adjuvant to improve anti-PD1 response in patients with CRC.

INTRODUCTION

The introduction of immune checkpoint blockade (ICB) therapy has revolutionised the paradigm of cancer treatment over the past decade. Harnessing the immune system, ICB therapy removes the 'brake' signal of T cell activation to elicit antitumour response.[1] ICB therapy, namely anti-PD1/PDL1 (programmed cell death protein 1/programmed death ligand 1) and anti-CTLA4 (cytotoxic T-lymphocyte-associated protein 4), has yielded great success in clinical trials and is now approved to treat different cancers.[2] Nevertheless, in colorectal cancer (CRC), clinical use of ICB therapy remains highly limited and is only approved in patients with high level of microsatellite instability (MSI-H) or mismatch repair deficiency, making up merely 15% of patients with CRC.[3] Meanwhile, drug resistance persists as an unresolved challenge—a large portion of patients, despite their eligibility to receive ICB, may be refractory or even fail to respond to anti-PD1 therapy.[4] Therefore, there is a dire need to identify

novel adjuvants to overcome ICB resistance and improve treatment efficacy.

The gut microbiota has emerged as an important factor dictating ICB response in various cancers. By metagenomic profiling, several studies reported a distinct microbiota composition between ICB responders and non-responders in patients with melanoma or epithelial cancer, while supplementing bacteria species enriched in responders or faecal microbiota transplantation to non-responders dramatically improved their ICB efficacy.[5–8] A recent study also demonstrated that a consortium of 11 bacterial strains from healthy donors effectively induced IFNγ^+CD8$^+$ T cells, which boosts antitumour immunity and synergised with ICB therapy.[9]

While earlier studies focus on the correlation between microbiota and host response, the underlying immunoregulatory mechanisms remain largely unknown. In view of this, recent publications have characterised several bacteria-derived immunomodulatory components, which are mostly bacterial metabolites or cell wall fragments such as inosine,[10] exopolysaccharides,[11] phospholipids[12] and peptidoglycan.[13] These findings have highlighted the potential of leveraging probiotics or bacteria-based therapeutics as an adjuvant to improve cancer immunotherapy.

We previously demonstrated that *Lactobacillus gallinarum*, a probiotic depleted in patients with CRC,[14] inhibited colorectal tumourigenesis by secreting indole-3-lactic acid (ILA), a tryptophan metabolite.[15] Tryptophan metabolites are known as a class of immunoregulatory metabolites, which could induce Th17 polarisation[16] and promote differentiation of CD4$^+$CD8$\alpha\alpha^+$ double-positive intraepithelial lymphocytes.[17] In this study, the translational potential of this probiotic beyond cancer prevention is explored—whether *L. gallinarum* may modulate antitumour immunity and improve ICB treatment in CRC. Our results showed that *L. gallinarum*-derived indole-3-carboxylic acid (ICA) significantly improved anti-PD1 therapy in CRC. ICA reduced regulatory T cell (Treg) infiltration and enhanced the effector function of CD8$^+$ T cells, mechanistically by modulating the indoleamine 2,3-dioxygenase 1 (IDO1)/Kynurenine (Kyn)/aryl hydrocarbon receptor (AHR) metabolic axis.

MATERIALS AND METHODS

Syngeneic mouse models

Male C57BL/6 or BALB/c mice at 5–6 weeks old were randomised and daily gavaged with (1) brain heart infusion (BHI) broth, (2) *Escherichia coli* MG1655 or (3) *L. gallinarum* (1×10^8 colony-forming unit/100 µL per mouse). After 1 week, MC38 (5×10^5 cells) or CT26 (1×10^6 cells) were subcutaneously injected into the dorsal flank of C57BL/6 or BALB/c mice, respectively. Alternatively, for adjuvant setting, bacterial gavage was started 3 days after tumour inoculation. When the tumour size reached 50–100 mm^3, anti-mouse PD1 monoclonal antibody (BE0146, Bio X Cell, Lebanon, New Hampshire, USA) or IgG isotype control (BE0089, Bio X Cell) was administered to mice by intraperitoneal injection every 3 days (100 µg per mouse). Tumour size was measured by calliper every 2–3 days.

For Treg depletion model, anti-mouse CD25 monoclonal antibody (BP0012, clone PC-61.5.3, Bio X Cell) was intraperitoneally injected to mice (150 µg per mouse) twice weekly, starting 1 week before tumour inoculation with four injections in total.

For *E. coli* mutant model, CT26 cells (1×10^6 cells) were inoculated on the dorsal flank of Balb/c mice. 3 days after tumour inoculation, *E. coli* MG1655 wild-type strain (*E. coli*-WT) or mutant strain (*E. coli*-ArAT) (1×10^8 colony-forming unit/100 µL per mouse) was gavaged to mice daily. Tumour inoculation and dosing schedule of anti-PD1 or isotype control are the same as described above.

For ICA model, ICA (10 mg/kg, Sigma-Aldrich, St. Louis, Missouri, USA) was gavaged to mice daily starting on day 3 after tumour inoculation. Tumour inoculation and dosing schedule of anti-PD1 or isotype control were the same as described above. After the outgrowth of palpable tumours, Kyn (10 mg/kg, Sigma-Aldrich) was intraperitoneally injected into mice twice weekly. For mice treated with AHR antagonist, CH-223191 (20 mg/kg, MedChemExpress LLC, Monmouth Junction, New Jersey, USA) was given to mice through oral gavage every day.

Germ-free mouse model

Germ-free mice were housed in germ-free animal facility at the First Affiliated Hospital, Sun Yat-sen University in Guangzhou, China. Germ-free male C57BL/6 mice at 5–10 weeks old were inoculated with MC38 cells (2×10^5 cells per tumour). After tumour injection, the mice were gavaged with phosphate-buffered saline or *L. gallinarum* (1×10^8 colony-forming unit) three times per week. When palpable tumours were observed, anti-PD1 monoclonal antibody or isotype control (100 µg per mouse) was given to mice by intraperitoneal injection every 3 days. The mice were euthanised and tumour tissues were collected on day 22.

Azoxymethane/dextran sulfate sodium-induced CRC model

Male C57BL/6 mice at 5–6 weeks old were intraperitoneally injected with a single dose of azoxymethane (AOM; Merck, Darmstadt, Germany), followed by 1 week of 1% dextran sulfate sodium (DSS; MP Biomedicals, Solon, Ohio, USA) in drinking water and a 2-week recovery period. A total of three DSS cycles were given. After the third DSS cycle, mice were randomised and gavaged with BHI broth, *E. coli* or *L. gallinarum* daily. For ICA model, we gavaged the mice with vehicle or ICA (18 mg/kg) per day, with or without intraperitoneal injection of Kyn (10 mg/kg) twice weekly. Anti-PD1 or isotype control (100 µg) were given to mice by intraperitoneal injection every 3 days after 1 week of bacterial gavage. Mouse colonoscopy (Karl Storz Endoskope, Tuttlingen, Germany) was performed before sacrifice.

All animal studies were approved by the Animal Experimentation Ethics Committee of The Chinese University of Hong Kong.

Bacterial strains and culture

L. gallinarum (ATCC 33199) was purchased from American Type Culture Collection (ATCC; Manassas, Virginia, USA). *E. coli* strain MG1655 was purchased from German Collection of Microorganisms and Cell Cultures GmbH (DSMZ) and is a non-pathogenic human commensal gut bacterium and was used as a negative control in this study. *L. gallinarum* and *E. coli* were cultured in MRS or BHI broth as appropriate in a shaking incubator at 37°C under aerobic condition, and were resuspended in BHI broth before gavage.

Cell lines and cell culture

Murine MC38 (microsatellite instability-high, MSI-H)[18] and CT26 (microsatellite stable)[19] and human (HCT116 and LoVo) CRC cell lines were purchased from ATCC. All cells were cultured in Dulbecco's modified Eagle's medium (Gibco BRL, Grand Island, New York, USA) supplemented with 10% fetal bovine serum and 1% penicillin/streptomycin, and maintained at 37°C in a humidified incubator with 5% carbon dioxide.

Statistical analysis

All results are expressed as mean±SD, unless otherwise indicated. Comparisons between two groups were performed using Mann-Whitney U tests. Kruskal-Wallis test was used to compare differences among multiple groups, and post hoc analysis was performed by Dunn's multiple comparison test. Two-way analysis of variance was used to determine statistical significance in tumour growth curve. Statistical tests were performed in GraphPad Prism (V.8.0, GraphPad Software, San Diego, California, USA). Two-tailed p values smaller than 0.05 were considered statistically significant.

Additional methods and details are provided in online supplemental methods and online supplemental tables S1–S3.

RESULTS

L. gallinarum improved anti-PD1 efficacy in syngeneic mouse models

To investigate whether *L. gallinarum* supplementation improves anti-PD1 efficacy, we first established a syngeneic mouse model by inoculating a murine MSI-H CRC cell line (MC38) into mice with daily gavage of either BHI (broth control), *E. coli* (bacterial negative control) or *L. gallinarum* (figure 1A). Once tumours were developed, anti-PD1 antibody or IgG isotype control was intraperitoneally injected to mice. *L. gallinarum* remarkably improved anti-PD1 efficacy, as evidenced by the reduced tumour size (figure 1B), tumour weight (figure 1C) and tumour volume (figure 1D), compared with anti-PD1 combined with BHI or *E. coli* control ($p<0.05$ for tumour weight, $p<0.01$ for tumour volume).

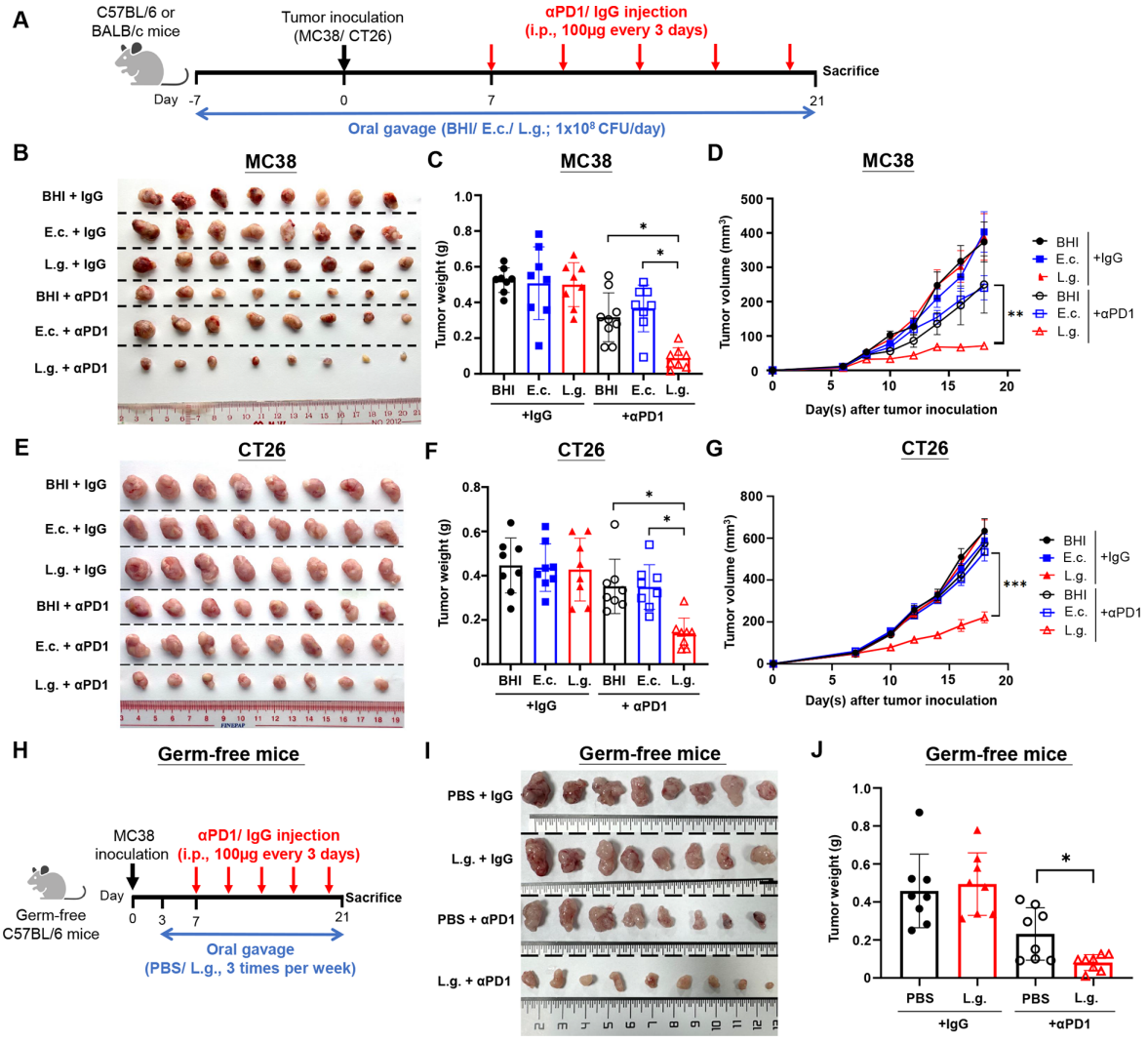

Figure 1 *Lactobacillus gallinarum* improved anti-PD1 efficacy in MC38 and CT26 syngeneic mouse models. (A) Schematic diagram of experimental design for syngeneic mouse model. *L. gallinarum*, in combination with anti-PD1 therapy, significantly inhibited tumour growth in MC38 syngeneic mouse model (microsatellite instability-high model), as evidenced by (B) representative tumour pictures, (C) tumour weight and (D) tumour volume. *L. gallinarum* also promoted anti-PD1 efficacy in CT26 syngeneic mouse model, an microsatellite instability-low model, as supported by (E) representative tumour pictures, (F) tumour weight and (G) tumour volume. (H) Schematic diagram of experimental design of germ-free mouse model. *L. gallinarum* mono-colonisation improved anti-PD1 efficacy in germ-free MC38 tumour-bearing mice, as shown by (I) representative tumour picture and (J) tumour weight. Statistical significance was determined by Kruskal-Wallis test, followed by Dunn's multiple comparison test. Statistical significance of tumour growth curve over time was determined by two-way analysis of variance. *p<0.05, **p<0.01, ***p<0.001. BHI, brain heart infusion; E.c., *E. coli*; L.g., *L. gallinarum*; PBS, phosphate-buffered saline; PD1, programmed cell death protein 1; αPD1, anti-PD1.

MC38 syngeneic model is a highly immunogenic model with good immunotherapy response.[18] We next sought to examine whether *L. gallinarum* could also be effective in a murine MSI-L CRC cell line (CT26), a model with inherited immunotherapy resistance.[19] As expected, anti-PD1 combined with BHI or *E. coli* showed minimal effects on tumour growth in CT26 syngeneic mice (figure 1E–G). In comparison, *L. gallinarum* supplementation significantly improved anti-PD1 efficacy, and the combination of anti-PD1 and *L. gallinarum* induced a marked reduction in tumour weight ($p<0.05$) (figure 1E,F) and tumour volume ($p<0.001$) (figure 1G). Altogether, these results suggested that *L. gallinarum* enhanced anti-PD1 efficacy to suppress tumour growth.

To explore the translational value of *L. gallinarum*, we validated our findings at an adjuvant setting, in which we started bacterial gavage 3 days after tumour inoculation, followed by anti-PD1 injection on day 7 (online supplemental figure 1A). Consistently, *L. gallinarum* supplementation improved anti-PD1 efficacy and reduced both tumour weight (both $p<0.01$) (online supplemental figure 1B,C) and tumour volume (both $p<0.05$) (online supplemental figure 1D). Our results suggested the potential of *L. gallinarum* as an adjuvant treatment for anti-PD1 therapy.

Next, we established a germ-free mouse model to validate whether *L. gallinarum* mono-colonisation could improve anti-PD1 efficacy in CRC (figure 1H). We confirmed that *L. gallinarum* mono-colonisation could improve anti-PD1 efficacy in germ-free MC38-tumour-bearing mice and significantly reduced tumour weight ($p<0.05$) (figure 1I,J). On top of being an additional phenotype validation, our results indicated that *L. gallinarum* was able to modulate antitumour immunity at a mono-colonisation setting, but not depending on the gut microbiota composition. We also confirmed *L. gallinarum* colonisation in the gut lumen, as evidenced by the detection of *L. gallinarum* in both stool and colon mucosa samples (online supplemental figure 1E) and the enrichment of *L. gallinarum* in colon mucosa samples after *L. galllinarum* gavage (online supplemental figure 1F).

L. gallinarum reduced Treg infiltration and enhanced effector function of $CD8^+$ T cells

Anti-PD1 efficacy is closely associated with immune cell infiltration. We therefore performed multicolour flow cytometric analysis and examined the change of immune landscape induced by *L. gallinarum* (online supplemental figure 2A). In MC38 syngeneic mouse model, *L. gallinarum* monotherapy, despite its inefficacy in impeding tumour growth, reduced $Foxp3^+CD25^+$ Treg infiltration, compared with BHI and *E. coli* group (both $p<0.05$) (figure 2A). In mice receiving *L. gallinarum* plus anti-PD1 therapy, we observed a consistent reduction of $Foxp3^+CD25^+$ Treg infiltration (both $p<0.05$), and also a significant induction of $IFN\gamma^+CD8^+$ T cells ($p<0.05$ for BHI; $p<0.01$ for *E. coli*) (figure 2B), which is an indicator of improved $CD8^+$ effector T cell function and strengthened antitumour immunity. We then validated our findings in the CT26 syngeneic mouse model. Consistently, *L. gallinarum* reduced Treg infiltration, both in monotherapy (both $p<0.05$) and combination with anti-PD1 therapy (both $p<0.01$) (figure 2A), and enhanced $IFN\gamma^+CD8^+$ T cells (both $p<0.001$) compared with BHI and *E. coli* controls (figure 2B). Further confirmation by immunohistochemistry (IHC) staining testified that $Foxp3^+$ cells were remarkably reduced in *L. gallinarum*-treated mice with or without anti-PD1 therapy (figure 2C and online supplemental figure 3A).

We also examined the change of other immune cells in tumour microenvironment (TME), including $CD8^+$ T cells (online supplemental figure 2B), $CD4^+$ T cells (online supplemental figure 2C), natural killer cells (online supplemental figure 2D) and myeloid-derived suppressor cells (online supplemental figure 2E). None of these immune cell components showed a significant change after *L. gallinarum* treatment in both syngeneic mouse models. Therefore, we considered that *L. gallinarum* improved anti-PD1 efficacy primarily by reducing Treg infiltration, which consequently remodelled the immunosuppressive TME and improved effector function of $CD8^+$ T cells. To testify these findings, we established a Treg depletion model by treating mice with anti-CD25 monoclonal antibody (online supplemental figure 3B). Flow cytometric analysis confirmed the successful Treg depletion in both tumour (online supplemental figure 3C) and plasma (online supplemental figure 3D). We found that anti-CD25 abolished the effect of *L. gallinarum* in promoting anti-PD1 efficacy, suggesting that the immunomodulatory effect of *L. gallinarum* was dependent on Treg suppression (figure 2D–F). Taken together, our results confirmed that *L. gallinarum* enhanced antitumour immunity by suppressing Treg intratumoural infiltration.

L. gallinarum sensitised mice to anti-PD1 therapy in AOM/DSS-induced CRC tumourigenesis model

To explore the translational potential of *L. gallinarum* in improving immunotherapy in CRC, we next established an AOM/DSS-induced CRC mouse model, which mimics physiological CRC development in humans. In contrast to our previous AOM/DSS model, which studied the cancer-preventive effect of *L. gallinarum* and sustained probiotic treatment throughout the tumourigenesis process,[15] we initiated *L. gallinarum* supplementation after the completion of three DSS cycles, 1 week before the start of anti-PD1 treatment, so as to better explore the role of *L. gallinarum* as a potential adjuvant to anti-PD1 (figure 3A). Consistent with the syngeneic mouse models, combining *L. gallinarum* and anti-PD1 significantly induced tumour shrinkage as evidenced by the colonoscopy images prior to sacrifice (figure 3B), and the representative colon images after sacrifice (figure 3C). Compared with anti-PD1-treated mice receiving BHI or *E. coli* control, *L. gallinarum* plus anti-PD1 therapy significantly reduced tumour number (both $p<0.01$) (figure 3D), tumour load (both $p<0.01$) (figure 3E) and number of large tumours (diameter ≥2 mm) ($p<0.05$ for BHI; $p<0.01$ for *E. coli*) (figure 3F), suggesting *L. gallinarum* boost the efficacy of anti-PD1 therapy against CRC. Colonic tumours were collected for immune cell analysis by flow cytometric. Consistent with the findings from syngeneic models, compared with anti-PD1-treated mice plus BHI or *E. coli* control, the combination of *L. gallinarum* and anti-PD1 significantly reduced Treg infiltration ($p<0.001$ for BHI; $p<0.01$ for *E. coli*) (figure 3G) and enhanced $CD8^+$ effector T cell function (both $p<0.05$) (figure 3H). Collectively, *L. gallinarum* synergised with anti-PD1 therapy in CRC treatment in mice.

L. gallinarum produced tryptophan as functional metabolites

L. gallinarum is known to be protective against colorectal tumourigenesis by producing antitumour metabolites.[15] We therefore characterised the metabolomic profile of *L. gallinarum* to identify functional metabolites that could modulate antitumour immunity. Untargeted metabolomic profiling revealed the significant enrichment of multiple tryptophan metabolites, including indole-3-carboxaldehyde (IAld), indoleacetic acid

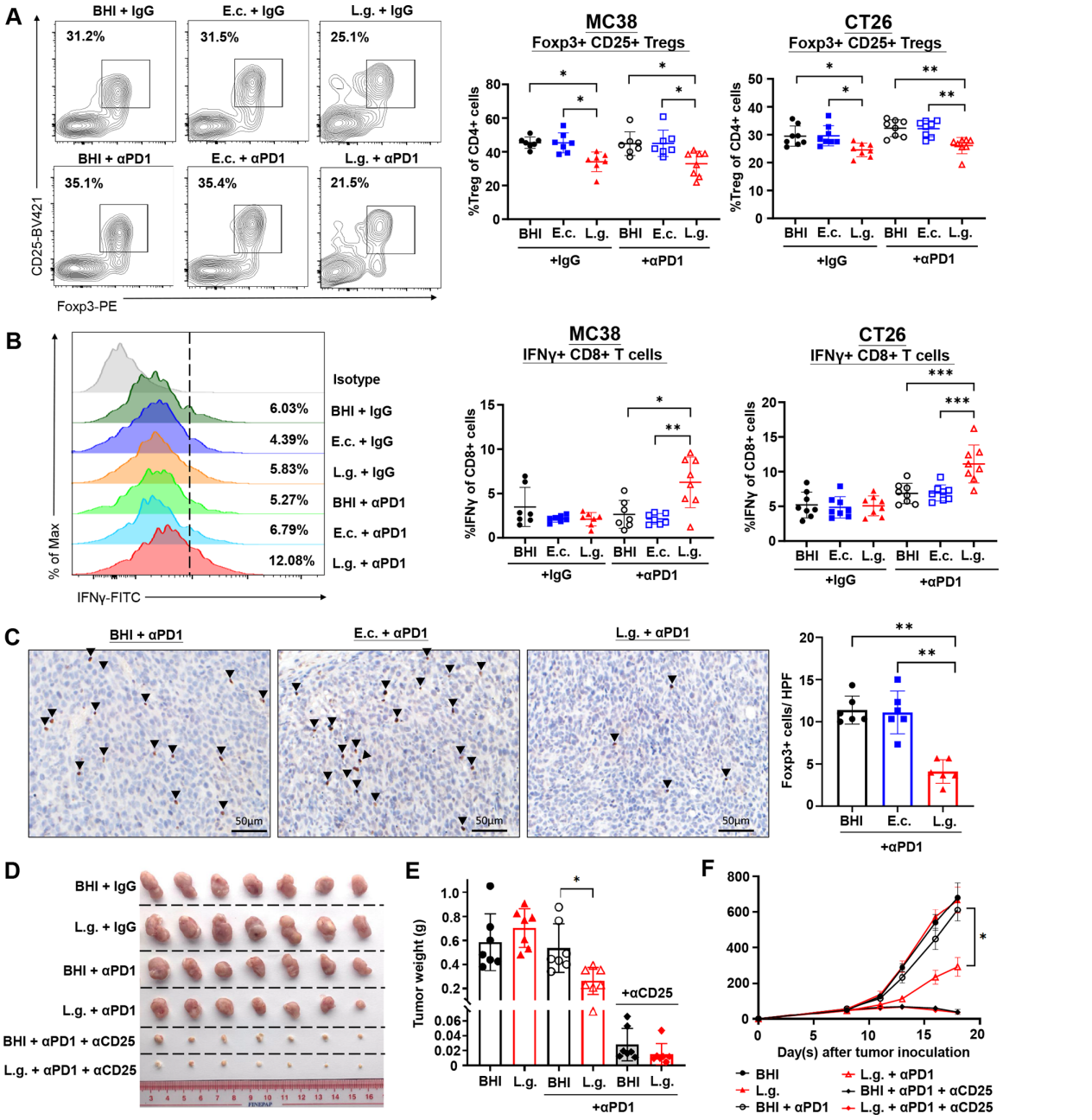

Figure 2 *Lactobacillus gallinarum* reduced Foxp3$^+$CD25$^+$ Treg infiltration and increased IFNγ$^+$CD8$^+$ T cells in the tumour microenvironment. (A) Representative flow cytometry plots of Foxp3$^+$ CD25$^+$ Treg suggested a significant reduction of Treg in tumour tissues of *L. gallinarum*-treated mice compared with that of BHI and *E. coli* controls. *L. gallinarum* significantly reduced Foxp3$^+$ CD25$^+$ Treg infiltration in MC38 tumours and CT26 tumours. (B) Representative histogram of IFNγ$^+$ CD8$^+$ T cells. Increased IFNγ$^+$ CD8$^+$ T cells were shown. in *L. gallinarum*, in combination with anti-PD1-treated MC38 tumours and CT26 tumours. (C) IHC staining confirmed a significant reduction of Foxp3$^+$ cells in *L. gallinarum*+anti-PD1-treated mice. The quantification of Foxp3$^+$ cells (the brown spot) was shown as the mean value of three independent HPF in tumours. Scale bar=50 μm. (D) Representative tumour pictures from the Treg depletion model. The administration of anti-CD25 monoclonal antibody abolished the effect of *L. gallinarum* in promoting anti-PD1 efficacy, as evidenced by (E) tumour weight and (F) tumour volume. Statistical significance was determined by Kruskal-Wallis test, followed by Dunn's multiple comparison test. Statistical significance of tumour growth curve over time was determined by two-way analysis of variance. *p<0.05, **p<0.01, ***p<0.001. E.c., *E. coli*; L.g., HPF, high-power fields; *L. gallinarum*; PD1, programmed cell death protein 1; Tregs, regulatory T cells; αCD25, anti-CD25; αPD1, anti-PD1.

(IAA) and indolelactic acid (ILA) in *L. gallinarum* culture supernatant (figure 4A). We then moved to the in vivo metabolomic profile and consistently observed an elevated faecal level of IAld in *L. gallinarum*-treated mice compared with BHI and *E. coli*-treated mice (figure 4B). For validation, we performed targeted metabolomic profiling on 32 different tryptophan-related metabolites (online supplemental table S4). Specifically, to examine the microbial tryptophan metabolism activity, we further selected 18 indole metabolites, which are the common tryptophan catabolites produced by gut bacteria. We examined the metabolomic profile of stool samples from MC38 syngeneic mouse model and confirmed a low tryptophan metabolism activity at baseline, while *L. gallinarum* administration induced a significant increase of microbial tryptophan metabolism and led to an enrichment

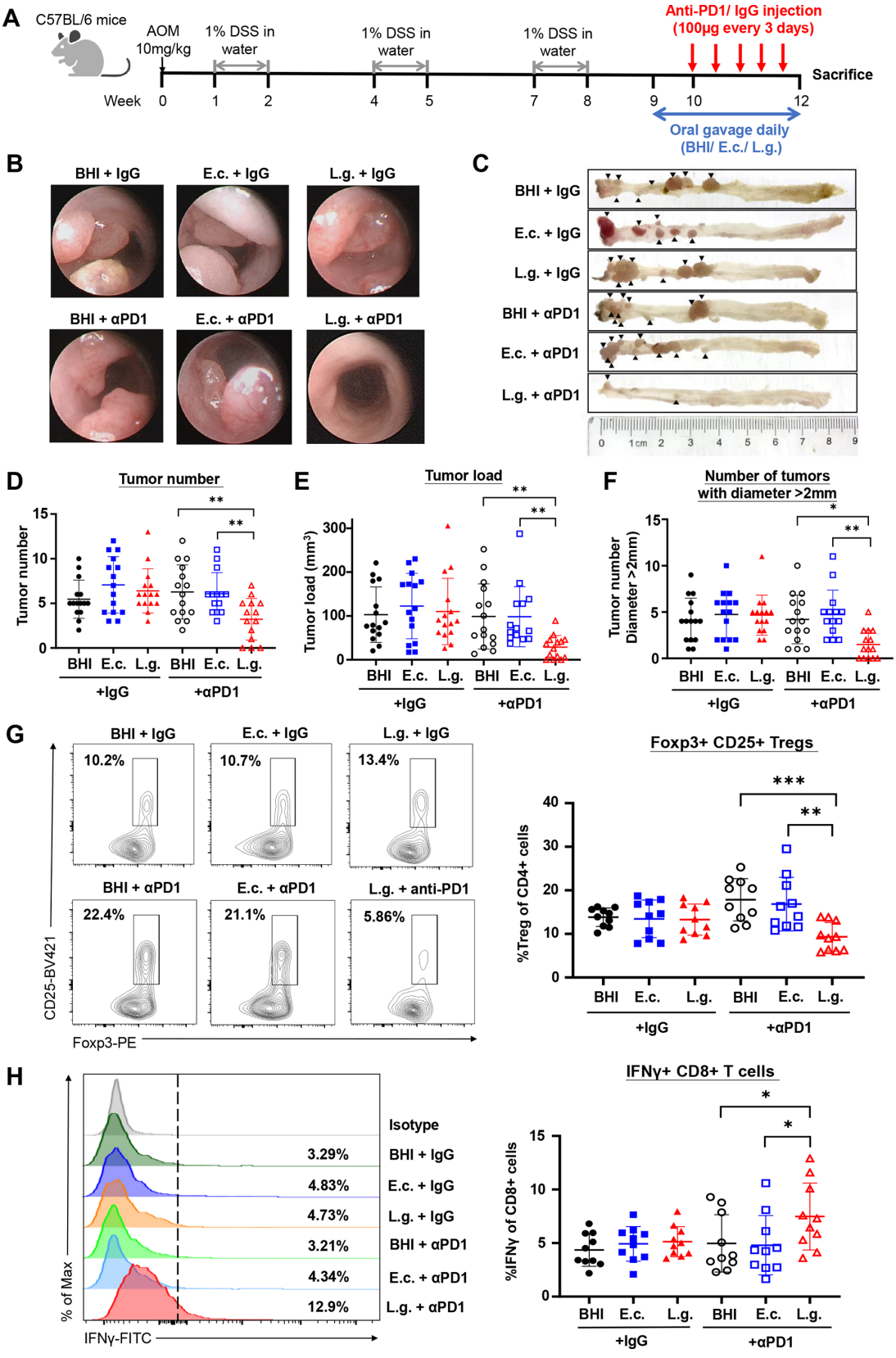

Figure 3 *Lactobacillus gallinarum* improved anti-PD1 efficacy in AOM/DSS-induced CRC mouse model. (A) Schematic diagram of experimental design for AOM/DSS-induced CRC model. (B) Representative colonoscopy images and (C) representative colon images of AOM/DSS-induced CRC tumourigenesis mouse model. *L. gallinarum*, in combination with anti-PD1, reduced (D) tumour number, (E) tumour load and (F) number of large tumours (diameter larger than 2 mm). (G) Percentage of $Foxp3^{+}CD25^{+}$ Tregs in colonic tumour tissues. (H) Percentage of $IFN\gamma^{+}$ $CD8^{+}$ T cells in colonic tumour tissues. Statistical significance was determined by Kruskal-Wallis test, followed by Dunn's multiple comparison test. *p<0.05, **p<0.01, ***p<0.001. AOM, azoxymethane; BHI, brain heart infusion; CRC, colorectal cancer; DSS, dextran sulfate sodium; E.c., *E. coli*; L.g., *L. gallinarum*; PD1, programmed cell death protein 1; Tregs, regulatory T cells; αPD1, anti-PD1.

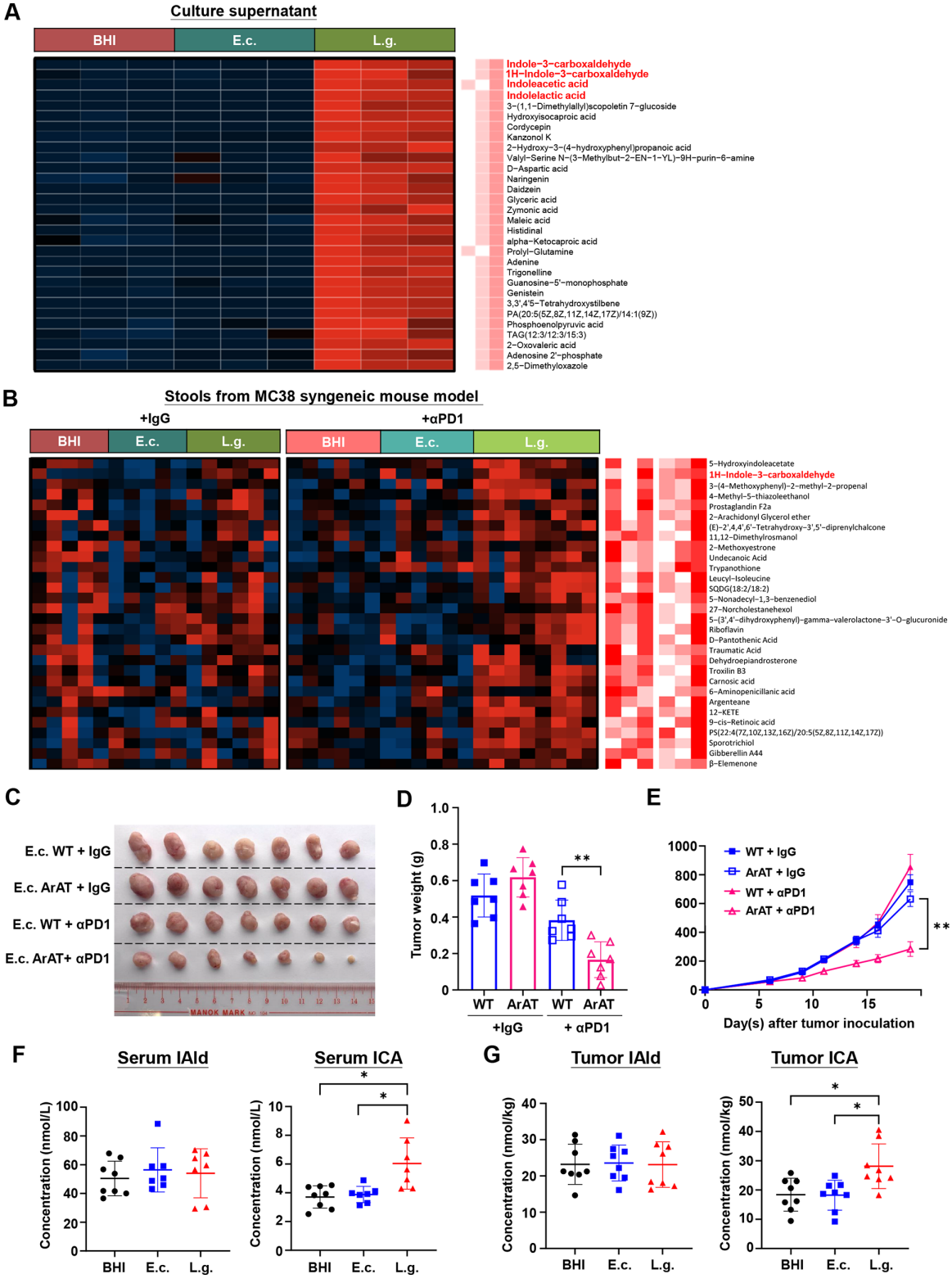

Figure 4 *Lactobacillus gallinarum* produced tryptophan metabolites in vitro and in vivo. (A) Untargeted metabolomics showing the heatmap analysis of BHI, *E. coli* and *L. gallinarum* culture supernatant in vitro. (B) Untargeted metabolomics showing heatmap analysis of stool samples from MC38 syngeneic mouse model revealed a differential abundance of metabolites in BHI-treated, *E. coli*-treated and *L. gallinarum*-treated mice. *E. coli* mutant expressing aromatic amino acid aminotransferase (*E. coli*-ArAT) improved ant-PD1 efficacy in CT26 syngeneic mouse model, as evidenced by (C) representative tumour picture, (D) tumour weight and (E) tumour volume. (F) No significant difference of IAld was observed in serum samples between groups. An elevated level of ICA was detected in serum after *L. gallinarum* gavage. (G) No significant difference of IAld was observed in tumour tissues between groups. ICA was enriched in tumour tissues of *L. gallinarum*-treated mice in MC38 syngeneic mouse model. Statistical significance was determined by Kruskal-Wallis test, followed by Dunn's multiple comparison test. Statistical significance of tumour growth curve over time was determined by two-way analysis of variance. *p<0.05, **p<0.01. ArAT, aromatic amino acid aminotransferase; E.c., *E. coli*; IAld, indole-3-carboxaldehyde; ICA, indole-3-carboxylic acid. L.g., *L. gallinarum*; WT, wild-type; αPD1, anti-PD1.

of indole metabolites (online supplemental figure 4A). In particular, IAld was significantly elevated in stool samples of *L. gallinarum*-treated mice ($p<0.05$ for BHI; $p<0.01$ for *E. coli*) (online supplemental figure 4B). These results suggested that *L. gallinarum* secreted tryptophan metabolites, specifically IAld, both in vitro and in vivo.

We then constructed an *E. coli* mutant strain expressing aromatic amino acid aminotransferase (ArAT) (*E. coli*-ArAT), which is the key bacteria enzyme for IAld synthesis[20] (online supplemental figure 4C,D), and gavaged to CT26 tumour-bearing mice daily. Compared with wild-type strain, *E. coli*-ArAT significantly improved anti-PD1 efficacy and reduced both tumour weight ($p<0.01$) and tumour volume ($p<0.01$) (figure 4C–E). Consistent with *L. gallinarum* model, we confirmed the elevated IAld level in stools (online supplemental figure 4E), as well as the suppression of Treg infiltration (online supplemental figure 4F) and enhanced effector function of $CD8^+$ T cells in tumour tissues of mice after *E. coli*-ArAT gavage (online supplemental figure 4G). These results strongly suggested that bacterial ArAT expression/IAld production would be one of the key players in modulating antitumour immunity and improving anti-PD1 efficacy.

Given that the tumours of syngeneic mice were located at their dorsal flank which were distant from the intestines, we hypothesised that *L. gallinarum*-derived metabolites were first produced in the gut, then entered the bloodstream and finally reached the tumour tissue. However, no significant difference of IAld level in serum and tumour tissues was found between groups (figure 4F,G), suggesting that IAld may not be the endpoint metabolite modulating antitumour immunity. In contrast, a significant enrichment of ICA, the downstream metabolite of IAld,[21] was observed in serum and tumour tissues of *L. gallinarum*-treated mice, compared with controls (both $p<0.05$) (figure 4F,G). Therefore, we postulated that *L. gallinarum* first produced IAld, the precursor of ICA in the gut, which was then converted to ICA in the bloodstream. ICA may be the functional metabolite that plays an immunoregulatory role.

L. gallinarum and ICA inhibited tumor IDO1 expression

In our metabolomic panel of tryptophan metabolites (online supplemental table S4), apart from elevated ICA level, we also observed a decreased Kyn level in both serum ($p<0.01$ for BHI; $p<0.05$ for *E. coli*) and tumour tissues (both $p<0.01$) of MC38 syngeneic mice with *L. gallinarum* treatment, compared with controls (figure 5A,B). A reduction of kynurenine-to-tryptophan (Kyn/Trp) ratio in tumour tissues of *L. gallinarum*-treated mice was also identified ($p<0.001$ for BHI; $p<0.05$ for *E. coli*) (figure 5C). Kyn is a host-derived metabolite notorious for promoting Treg development and immune evasion, and is primarily produced by indoleamine 2,3-dioxygenase (IDO) through tryptophan conversion.[22] Based on these findings, we hypothesised that *L. gallinarum* suppressed IDO expression and/or activity in tumours, which subsequently reduced Kyn production.

We therefore performed RNA sequencing on tumour tissues from MC38 syngeneic mouse model (figure 5D). The tryptophan metabolism pathway was significantly downregulated in mice with cotreatment of *L. gallinarum* and anti-PD1, compared with BHI plus anti-PD1 and *E. coli* plus anti-PD1 groups (both $p<0.05$) (figure 5E). To validate the sequencing results, we confirmed the reduced IDO1 expression in tumour tissues of syngeneic mice by IHC staining ($p<0.001$ for BHI; $p<0.01$ for *E. coli*) (figure 5F). Consistently, the mRNA expression (online supplemental figure 5A) and protein expression (online supplemental figure 5B) of IDO1 in tumour tissues of syngeneic mouse models was significantly reduced after *L. gallinarum* treatment. These results suggested that *L. gallinarum* suppressed IDO1 expression and reduced Kyn production in tumour tissues.

Given that ICA was identified as the functional metabolite of *L. gallinarum* (figure 4), we postulated that ICA could be an IDO1 inhibitor. Indeed, ICA significantly suppressed IDO1 expression in two human CRC cell lines (HCT116 and LoVo) at both mRNA (online supplemental figure 5C) and protein level (figure 5G), and this was further confirmed by the reduced Kyn in cell lysates using liquid chromatography-mass spectrometry (LC-MS) analysis (figure 5H). Taken together, these results indicated that *L. gallinarum* and ICA inhibited IDO1 expression and reduced Kyn production in tumours.

ICA antagonised Kyn-mediated Treg differentiation by inhibiting AHR activation

To explore the impact of *L. gallinarum*-derived metabolites on Treg differentiation, we treated naïve $CD4^+$ T cells with *L. gallinarum* culture supernatant, IAld or ICA. However, none of these treatments had significant effects on Treg differentiation, hinting an indirect effect of ICA on Treg differentiation (figure 6A and online supplemental figure S6A,B). ICA and other tryptophan metabolites, including Kyn, are known to activate AHR,[23] whereas AHR activation is associated with Treg differentiation and immune escape.[24] Therefore, we hypothesised that ICA may compete with Kyn, a host-derived AHR agonist highly enriched in tumour tissues,[25] and consequently antagonised Kyn-mediated AHR activation. We simultaneously treated $CD4^+$ T cells with Kyn and ICA. Kyn (50 µM) significantly induced Treg differentiation ($p<0.0001$), while the addition of ICA, at a much lower dose (as low as 1.25 µM), antagonised Kyn-mediated Treg differentiation in a dose-dependent manner (figure 6B). We then measured the expression of AHR target gene CYP1B1 on $CD4^+$ T cells. ICA alone weakly promoted CYP1B1 expression, suggesting ICA as a weak AHR agonist (figure 6C). In contrast, Kyn-induced CYP1B1 expression was markedly suppressed by the addition of ICA to Kyn. The use of CH-233191, an AHR antagonist, also abolished both Kyn and ICA effects in mediating Treg differentiation (figure 6D). These results therefore revealed that ICA could inhibit Kyn-induced AHR activation.

On the other hand, we also examined the effect of ICA and Kyn on functions of $CD4^+$ and $CD8^+$ T cells to explore the potential of any non-specific effects induced by ICA and/or Kyn. We demonstrated that ICA has no effect on the effector function of $CD8^+$ T cells (online supplemental figure S6C), Th1 or Th2 $CD4^+$ T cell polarisation (online supplemental figure S6D,E). Kyn has negligible effect of Th1 or Th2 $CD4^+$ T cell differentiation (online supplemental figure S6D,E), while consistent with previous literature,[26] Kyn suppressed the portion of $IFN\gamma^+$ $CD8^+$ T cells at high dose (200 µM) (online supplemental figure 6C). Therefore, we confirmed that the effect of ICA and Kyn (at low dose, eg, 50 µM) is $CD4^+$ T cell-specific/ Treg-specific.

We then examined how ICA interacts with AHR by in silico analysis. Molecular docking analysis showed that ICA binds to the ligand-binding domain (LBD) of AHR protein and shares a similar binding site with Kyn (figure 6E). The binding of ICA on AHR receptor resulted in similar

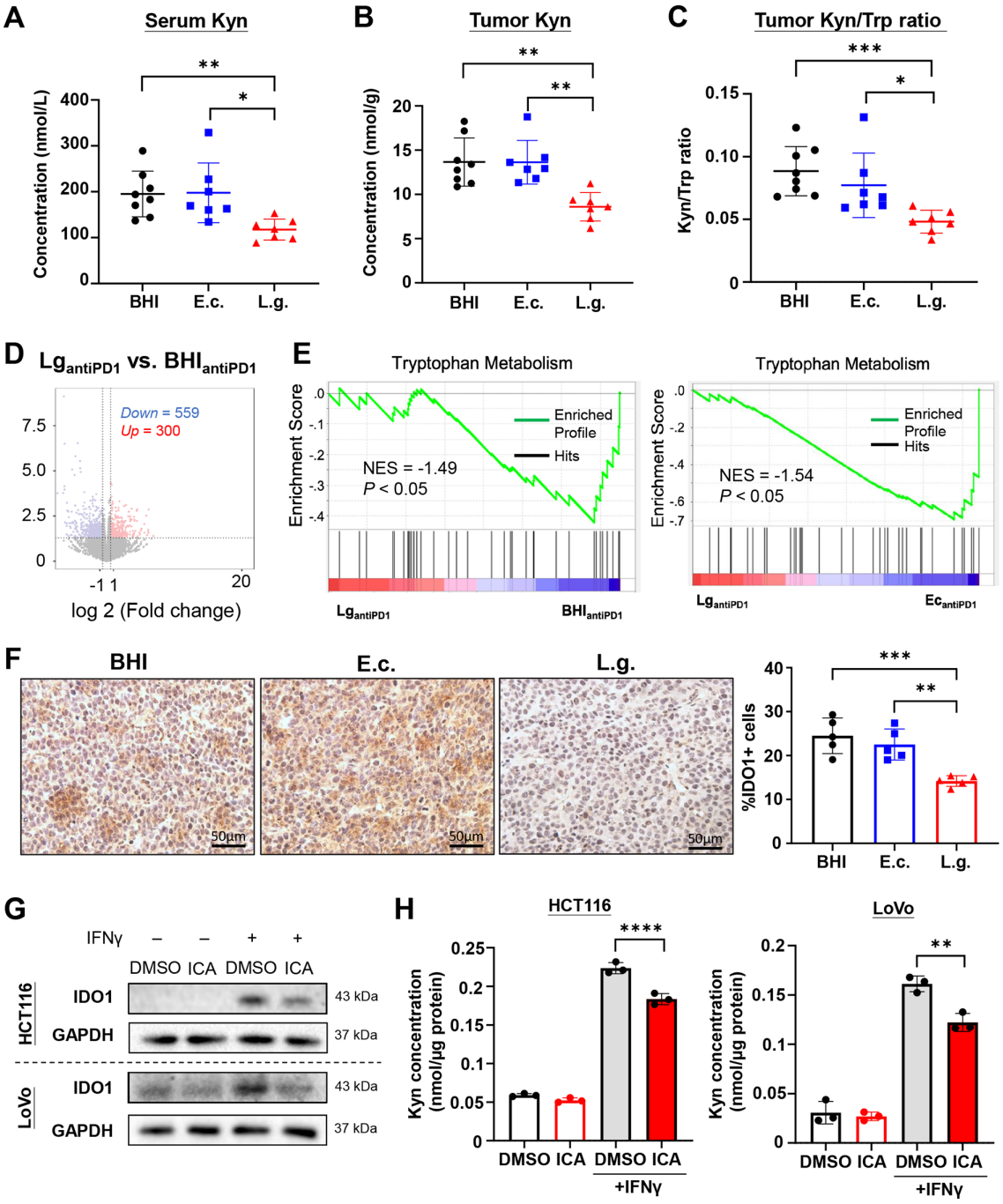

Figure 5 *Lactobacillus gallinarum* and ICA inhibited IDO1 expression and Kyn production in tumour. *L. gallinarum* reduced (A) serum Kyn level, (B) tumour Kyn level, (C) Kyn/Trp ratio in tumours in MC38 syngeneic mouse model. (D) RNA sequencing revealed a differential gene expression between BHI plus anti-PD1 group versus *L. gallinarum* plus anti-PD1 group. (E) Enrichment plot of Trp metabolism pathway. (F) Immunohistochemical staining of IDO1 in tumour tissues of CT26 syngeneic mouse model. Scale bar=50 μm. (G) ICA (5 μM) significantly inhibited IDO1 expression in HCT116 and LoVo cell lines. IFNγ (100 ng/mL) was added 1 day after ICA/DMSO treatment to induce IDO1 expression. (H) ICA (5 μM) reduced Kyn level in HCT116 and LoVo cell lysates, as detected by Liquid chromatography-mass spectrometry, after normalisation of protein concentration. IFNγ (100 ng/mL) was added to induce IDO1 expression. Statistical significance was determined by Kruskal-Wallis test, followed by Dunn's multiple comparison test. *p<0.05, **p<0.01, ***p<0.001, ****p<0.0001. E.c., *E. coli*; ICA, indole-3-carboxylic acid; IDO1, indoleamine 2,3-dioxygenase; Kyn, kynurenine; L.g., *L. gallinarum*; Trp, tryptophan.

binding energy (−6.654 kcal/mol) as that between Kyn and AHR (−6.985 kcal/mol), suggesting a comparable binding or conformation stability between ICA and Kyn towards AHR. We further examined the ligand–protein interaction by surface plasmon resonance (SPR) assay. Both ICA and Kyn could bind to AHR, while ICA had a lower dissociation constant (KD) (39.4 μM) than Kyn (61.5 μM), indicating a higher receptor affinity to AHR (figure 6F). These results have therefore suggested the possibility of receptor competition between the two metabolites.

To explore the kinetic mechanism, we constructed a Lineweaver-Burk plot by treating mouse T cells with various

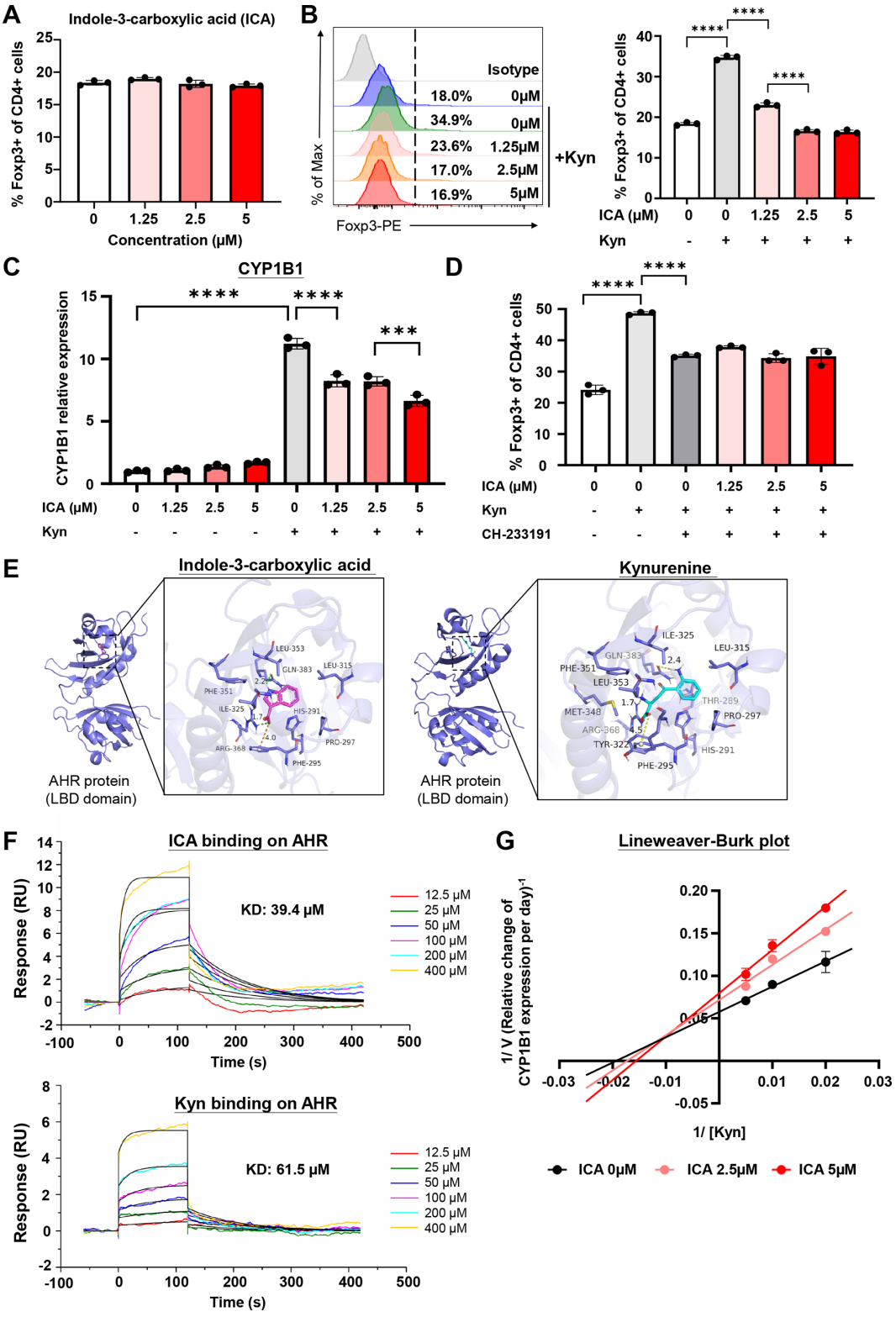

Figure 6 ICA outcompeted Kyn and inhibited Kyn-mediated AHR activation on CD4+T cells. (A) ICA did not directly affect Treg differentiation in vitro. (B) Effect of ICA and Kyn (50 μM) on Foxp3^{+}Treg differentiation. ICA antagonised Kyn-mediated Treg differentiation in a dose-dependent manner. (C) CYP1B1 expression of CD4+T cells treated with different doses of ICA and Kyn (50 μM). ICA significantly inhibited Kyn-mediated upregulation of CYP1B1 expression. (D) CH-233191 (AHR antagonist) (10 μM) abolished the effect of ICA and Kyn. (E) Molecular docking analysis of ICA and Kyn on LBD of human AHR protein. ICA bound to the LBD of AHR protein with a binding energy of −6.654 kcal/mol. Kyn bound to the LBD of AHR protein with a binding energy of −6.985 kcal/mol. (F) SPR assay of ICA and Kyn on human AHR protein. ICA has a higher receptor affinity to AHR compared with Kyn (KD: 39.4 μM vs 61.5 μM). (G) Lineweaver-Burk plot was constructed by treating mouse T cells with various dosages of ICA and Kyn. Reaction velocity (V) is defined as the relative change of CYP1B1 expression per day. Statistical significance was determined by Kruskal-Walli test, followed by Dunn's multiple comparison test. ***p<0.001, ****p<0.0001. AHR, aryl hydrocarbon receptor; ICA, indole-3-carboxylic acid; KD, dissociation constant; Kyn, kynurenine; LBD, ligand-binding domain; SPR, surface plasmon resonance.

doses of ICA and Kyn[27 28] (figure 6G). The increase of x-intercept (defined as −1/Km, whereas Km stands for the Michaelis constant) indicated an increase in Km and therefore the presence of competitive inhibition. Nevertheless, we note that the antagonising activity of Kyn is a mixed mode of inhibition that both competitive and non-competitive inhibition existed—this was evidenced by the increase of y-intercept (defined as 1/Vmax, where Vmax stands for the limiting rate of the system), suggesting the decrease of Vmax and the presence of non-competitive inhibition. Taken together, we confirmed that ICA inhibited AHR activation at least partially as a competitive AHR inhibitor. Cumulatively, ICA directly bound to AHR receptor on CD4$^+$ T cells, thereby antagonising Kyn-mediated AHR activation and subsequent Treg differentiation.

ICA phenocopied *L. gallinarum* effect in vivo, and was reversed by Kyn supplementation

To confirm the effect of ICA in modulating antitumour immunity, we established a CT26 syngeneic mouse model with daily gavage of ICA with or without anti-PD1. ICA significantly promoted anti-PD1 efficacy and phenocopied the effect of *L. gallinarum*, as evidenced by the reduced tumour weight and tumour volume

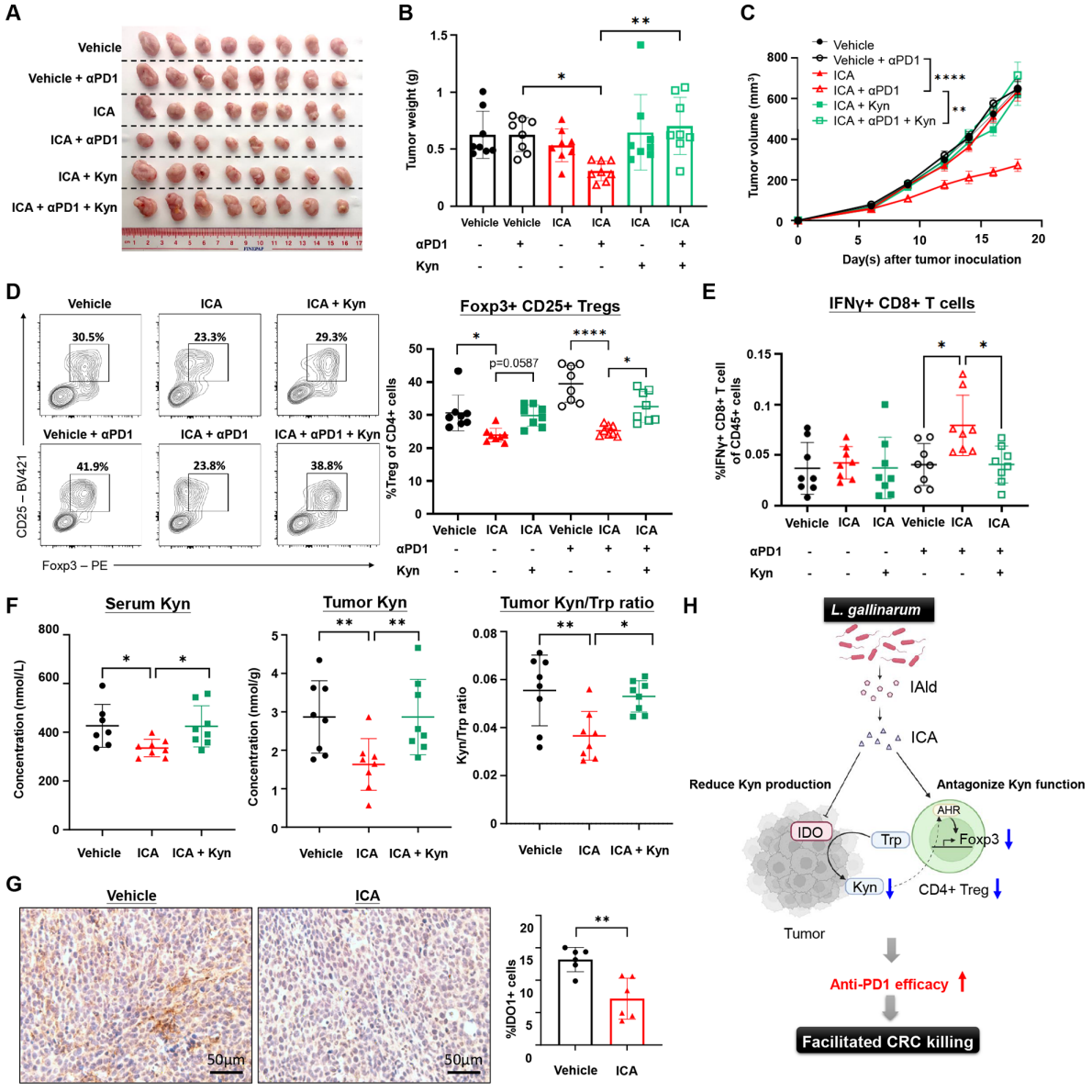

Figure 7 ICA improved anti-PD1 efficacy and was rescued by Kyn supplementation. ICA in combination with anti-PD1 impeded tumour growth, as evidenced by (A) representative tumour picture, (B) tumour weight and (C) tumour volume in CT26 syngeneic mouse model. (D) ICA reduced Foxp3$^+$ CD25$^+$ infiltration in tumour tissues, which was reversed by Kyn supplementation. (E) ICA increased the proportion of IFNγ$^+$ CD8$^+$ T cells in tumour tissues, which was reversed by Kyn supplementation. (F) ICA reduced Kyn level in serum and tumour tissues, and decreased Kyn/Trp ratio in tumour tissues, which was reversed by Kyn supplementation. (G) Immunohistochemistry staining revealed that ICA reduced IDO1 expression in tumour tissues. Scale bar=50 μm. (H) Schematic diagram outlining the mechanistic pathway of how *L. gallinarum* improved anti-PD1 efficacy in colorectal cancer. Statistical significance was determined by Mann-Whitney U test or Kruskal-Wallis test, followed by Dunn's multiple comparison test, where appropriate. Statistical significance of tumour growth curve over time was determined by two-way analysis of variance. *p<0.05, **p<0.01, ****p<0.0001. ICA, indole-3-carboxylic acid; Kyn, kynurenine; Tregs, regulatory T cells; Trp, tryptophan; αPD1, anti-PD1.

compared with vehicle control, while Kyn supplementation reversed the effect of ICA (figure 7A–C). Oral gavage of ICA resulted in a significant increase of ICA level in stools, serum and tumour tissues, confirming the enrichment of ICA in vivo after oral administration (online supplemental figure 7A). We then further confirmed the effect of ICA and Kyn in an AOM/DSS-induced CRC model and demonstrated that ICA significantly improved therapeutic efficacy of anti-PD1 and induced tumour shrinkage, as evidenced by the colonoscopy and representative colon images (online supplemental figure 7B,C), as well as the remarkable reduction in tumour number (online supplemental figure S7D), tumour load (online supplemental figure S7E) and number of large tumours (≥2 mm) (online supplemental figure S7F), which was antagonised by Kyn supplementation.

Consistent with the results of *L. gallinarum*-treated mice (figure 2), ICA significantly reduced Treg infiltration (figure 7D) and increased IFNγ$^+$CD8$^+$ T cells (figure 7E) in tumour tissues, which was also reversed by Kyn supplementation. ICA treatment also reduced Kyn level in serum and tumour tissues, as well as the Kyn/Trp ratio in tumours (figure 7F). IHC staining further confirmed the reduced IDO1 expression in ICA-treated tumour tissues ($p<0.01$) (figure 7G), which further corroborated with our hypothesis that *L. gallinarum* or ICA modulated antitumor immunity through modulating the IDO1/Kyn axis.

To validate the mechanistic importance of AHR signalling in ICA-mediated effects, we next established a MC38 syngeneic mouse model and treated the mice with CH-223191 (AHR antagonist). Consistent with CT26 model, ICA improved anti-PD1 efficacy in MC38 syngeneic mouse model, as evidenced by the reduced tumour weight ($p<0.01$) (online supplemental figure 7G) and tumour volume ($p<0.05$) (online supplemental figure 7H). The use of CH-223191 abolished the effect of ICA promoting anti-PD1 efficacy (figure 7G,H), suggesting that ICA improved anti-PD1 response by inhibiting AHR activation. Flow cytometric analysis confirmed a reduction of Foxp3$^+$ CD25$^+$ Tregs and an increase of IFNγ$^+$ CD8$^+$ T cells, which were both abolished after CH-223191 treatment (online supplemental figure 7I, J).

Collectively, our results demonstrated that *L. gallinarum* and its derived ICA improved anti-PD1 therapy in a two-fold mechanism: (1) inhibiting IDO1 expression and Kyn production, and (2) inhibiting Kyn binding on AHR through receptor competition (figure 7H).

DISCUSSION

In this study, we reported that *L. gallinarum* supplementation sensitised mice to anti-PD1 therapy in both syngeneic and CRC tumourigenesis mouse models. Our results illustrated a novel metabolic mechanism of how a probiotic species modulated antitumour immunity and improved ICB response. Particularly, we identified ICA, a tryptophan metabolite secreted by *L. gallinarum*, as the key player in remodelling TME through modulating the IDO1/Kyn/AHR metabolic axis.

We first demonstrated that *L. gallinarum* significantly augmented anti-PD1 efficacy and induced a remarkable tumour shrinkage. Accumulating evidence suggested that gut microbiota composition shapes the outcome of cancer immunotherapy, while microbiota modulation arises as a promising approach to improve ICB response. We revealed that *L. gallinarum* reduced Foxp3$^+$CD25$^+$ Treg infiltration in TME and enhanced effector function of CD8$^+$ T cells when combined with anti-PD1, indicating the strengthened antitumour immunity. Notably, *L. gallinarum* was effective in improving anti-PD1 efficacy in CT26 syngeneic mouse model, an MSI-low model known to have minimal response to immunotherapy. Treg recruitment and infiltration is one of the key mechanisms accounting for ICB resistance, which contributed to the immunosuppressive TME and prevented the cytotoxic activities of effector T cells.[29] Meanwhile, to better mimic human CRC development, we established a carcinogen AOM/DSS-induced CRC mouse model and revealed that *L. gallinarum* also significantly improved anti-PD1 therapy with a marked reduction of tumour growth. In supporting our identification, a recent study reported that probiotic *Lactobacillus acidophilus* improved ICB efficacy by reducing intratumoural Treg and enhancing effector CD8$^+$ T cells.[30] Taken together, our results from different mouse models suggested an immense translational potential of leveraging probiotic *L. gallinarum* in reshaping the immunosuppressive TME and reversing ICB resistance in clinical practice.

Through metabolomic profiling and biological validation, we identified ICA as the functional immunomodulatory component that improved anti-PD1 therapy. We initially focused on IAld, given its enrichment in *L. gallinarum* culture supernatant and stool samples of *L. gallinarum*-treated mice. However, metabolomic analysis revealed no significant difference in serum IAld level. Instead, a significant enrichment of ICA, the downstream metabolite of IAld, was observed between *L. gallinarum* and control groups. Therefore, we reasoned that *L. gallinarum* first produced IAld, which was converted to ICA after entering the bloodstream, and ICA functioned as the endpoint metabolite that modulated antitumour immunity. The indole pathway in host and bacteria is known to be a highly dynamic process, which is characterised by rapid biotransformation and biodegradation of various indole metabolites in vivo. While ICA is reported to be a direct downstream metabolite of IAld,[21] and the conversion from IAld to ICA only involves a single oxidation step, we therefore posited that the conversion could be driven by the cytochrome P450 enzymes in the liver,[31] which have been reported to engage in biotransformation of indole metabolites in vivo.[32] Meanwhile, taking accounting into the key role of gut microbiota in tryptophan and indole metabolism, other gut commensal bacteria may also be potential candidates responsible for the IAld conversion.[31] To this end, we strongly believe that such IAld-to-ICA conversion was physiologically plausible, given the simplicity of conversion step, as well as the documented presence of host/bacterial catalysts.

Mechanistically, we revealed that *L. gallinarum* and its derived ICA regulated the host tryptophan metabolism pathway and inhibited IDO1 expression in tumour tissues, leading to a reduced production of Kyn, a host-derived metabolite contributing to tumour progression, immune escape and Treg development.[25] The conversion of tryptophan to Kyn is regulated by IDO1, which is highly expressed in multiple human cancers and has been an attractive pharmaceutical target.[33] In line with our observations, several studies have reported the role of probiotics in inhibiting IDO1 expression and lowering Kyn concentration in vivo.[34 35] Kyn/Trp ratio is also known to be a prognosis marker predicting ICB response.[36] Here we reported an effector mechanism of how the gut microbiota modulated ICB response through host-bacteria metabolic crosstalk. In general, tryptophan metabolism involves three major pathways which are modulated by host, epithelial/immune cells and enterochromaffin cells, respectively,[37] while modulation of one of these metabolic pathways profoundly disturb the others.[38] Collectively, our results suggested that *L. gallinarum* and its derived ICA, exert the immunomodulatory effect, at least in part, by modulating the host tryptophan metabolism pathway and inhibiting Kyn production in TME.

Apart from interfering with the upstream IDO1 enzyme, we also reported a downstream mechanism involving a receptor competition between ICA and Kyn for the binding site of AHR on T cells, which subsequently inhibited Treg differentiation. We found that *L. gallinarum*-derived ICA or IAld had insignificant immunomodulatory effects on Treg differentiation, suggesting that ICA improved ICB response through an indirect manner. Indeed, our results confirmed that ICA could suppress Kyn-mediated Treg differentiation through an AHR-dependent manner. Tryptophan metabolites including both indoles and Kyn are widely reported as AHR-binding ligands.[39] Several studies reported the antagonistic activity of indole metabolites—while indole metabolites alone function as a weak AHR agonist, they also exhibited antagonistic activity and inhibited agonist-induced AHR activation.[23] AHR agonists or indole metabolites are known to play a pleiotropic role in cancer. For instance, although AHR agonists could alleviate colonic inflammation and thus potentially prevent colitis-associated CRC,[40 41] they may in turn promote immune evasion in TME in established cancer.[42 43] *Lactobacillus*-derived indole metabolites were recently reported to drive immunosuppression by activating AHR on tumour-associated macrophages to promote tumour progression.[43] In our study, we demonstrated a competitive nature between host- and microbiota-derived AHR ligands, showing that *L. gallinarum*-derived ICA (a weak AHR agonist) outcompeted Kyn and inhibited Kyn-mediated AHR activation. In fact, the use of partial agonist is not a rare concept in drug development. Several drug classes in clinical use today, such as opioids (for chronic pain relief)[44] and beta-blockers (for treating cardiovascular disease),[45] also include members with partial agonistic activity. Compared with pure antagonists, partial agonists also prevent full receptor activation, but at the same time maintain physiological homeostasis. Our results collectively suggested that gut microbiota-derived AHR ligands function as a partial AHR agonist and a competitive AHR inhibitor, which suppress AHR activation in TME under the presence of host-derived AHR ligands.

Of note, one of the limitations of this study is the potential gap between our in vitro and in vivo findings. We noticed a discrepancy of ICA dose in our in vitro investigations and in vivo metabolomic analysis—although we observed consistent pharmacodynamic changes including reduced Treg infiltration, reduced Kyn level and inhibited IDO1 expression after ICA or *L. gallinarum* gavage, we cannot exclude the possibility that other molecular mechanisms may underlie the animal phenotype. To address this concern, further pharmacokinetic investigations, including the absorption, distribution, metabolism and excretion properties of ICA and other metabolites, may be warranted.

In conclusion, we demonstrated that *L. gallinarum* and its derived ICA could improve anti-PD1 efficacy in CRC. Such actions are associated with the inhibition of IDO1/Kyn metabolic circuit, as well as the antagonism of Kyn binding to AHR receptors on T cells to inhibit Treg differentiation (figure 7H). Altogether, our results describe a novel mechanism underlining the host-microbiota metabolic crosstalk and highlight the translational potential of leveraging *L. gallinarum* as an adjuvant therapy to improve ICB response in patients with CRC.

Author affiliations
[1]Institute of Digestive Disease, Department of Medicine and Therapeutics, State Key Laboratory of Digestive Disease, Li Ka Shing Institute of Health Sciences, The Chinese University of Hong Kong, Hong Kong, China
[2]Department of Anaesthesia and Intensive Care and Peter Hung Pain Research Institute, The Chinese University of Hong Kong, Hong Kong, China
[3]Institute of Precision Medicine, The First Affiliated Hospital of Sun Yat-Sen University, Guangzhou, China
[4]School of Pharmacy, The Chinese University of Hong Kong, Hong Kong, China
[5]Lee Kong Chian School of Medicine, Nanyang Technological University, Singapore

Contributors WF performed experiments and drafted the manuscript. QL performed the experiments and revised the manuscript. HCHL revised the manuscript. FJ, WLiang, XK performed the experiments. WLiu performed bioinformatic analyses. KKT, ZZ, XZ and JJYS supervised and commented on the study. JY designed and supervised the study and revised the manuscript. JY is guarantor of the manuscript.

Funding This project was supported by Research Talent Hub-Innovation and Technology Fund Hong Kong (ITS/177/21FP); RGC Research Impact Fund Hong Kong (R4032-21F); Shenzhen-Hong Kong-Macao Science and Technology Program (Category C) Shenzhen (SGDX20210823103535016).

Competing interests None declared.

Patient and public involvement Patients and/or the public were not involved in the design, or conduct, or reporting or dissemination plans of this research.

Patient consent for publication Not applicable.

Ethics approval Not applicable.

Provenance and peer review Not commissioned; externally peer reviewed.

Data availability statement All data relevant to the study are included in the article or uploaded as supplementary information.

ORCID iDs
Harry Cheuk Hay Lau http://orcid.org/0000-0003-3581-2909
Xiaoxing Li http://orcid.org/0000-0001-8791-7505
Joseph JY Sung http://orcid.org/0000-0003-3125-5199
Jun Yu http://orcid.org/0000-0001-5008-2153

REFERENCES

1 Wei SC, Duffy CR, Allison JP. Fundamental mechanisms of immune checkpoint blockade therapy. *Cancer Discov* 2018;8:1069–86.
2 Ribas A, Wolchok JD. Cancer immunotherapy using checkpoint blockade. *Science* 2018;359:1350–5.
3 André T, Shiu K-K, Kim TW, *et al*. Pembrolizumab in microsatellite-instability–high advanced colorectal cancer. *N Engl J Med* 2020;383:2207–18.
4 Sahin IH, Akce M, Alese O, *et al*. Immune checkpoint inhibitors for the treatment of MSI-H/MMR-D colorectal cancer and a perspective on resistance mechanisms. *Br J Cancer* 2019;121:809–18.
5 Gopalakrishnan V, Spencer CN, Nezi L, *et al*. Gut microbiome modulates response to anti-PD-1 immunotherapy in melanoma patients. *Science* 2018;359:97–103.
6 Routy B, Le Chatelier E, Derosa L, *et al*. Gut microbiome influences efficacy of PD-1-based immunotherapy against epithelial tumors. *Science* 2018;359:91–7.
7 Sivan A, Corrales L, Hubert N, *et al*. Commensal bifidobacterium promotes antitumor immunity and facilitates anti-PD-L1 efficacy. *Science* 2015;350:1084–9.
8 Davar D, Dzutsev AK, McCulloch JA, *et al*. Fecal microbiota transplant overcomes resistance to anti-PD-1 therapy in melanoma patients. *Science* 2021;371:595–602.
9 Tanoue T, Morita S, Plichta DR, *et al*. A defined commensal consortium elicits CD8 T cells and anti-cancer immunity. *Nature* 2019;565:600–5.
10 Mager LF, Burkhard R, Pett N, *et al*. Microbiome-derived Inosine modulates response to checkpoint inhibitor immunotherapy. *Science* 2020;369:1481–9.
11 Kawanabe-Matsuda H, Takeda K, Nakamura M, *et al*. Dietary lactobacillus-derived exopolysaccharide enhances immune-checkpoint blockade therapy. *Cancer Discov* 2022;12:1336–55.
12 Bae M, Cassilly CD, Liu X, *et al*. Akkermansia muciniphila phospholipid induces homeostatic immune responses. *Nature* 2022;608:168–73.
13 Griffin ME, Espinosa J, Becker JL, *et al*. Enterococcus peptidoglycan remodeling promotes checkpoint inhibitor cancer immunotherapy. *Science* 2021;373:1040–6.

14 Dai Z, Coker OO, Nakatsu G, *et al*. Multi-cohort analysis of colorectal cancer metagenome identified altered bacteria across populations and universal bacterial markers. *Microbiome* 2018;6:70.
15 Sugimura N, Li Q, Chu ESH, *et al*. *Lactobacillus Gallinarum* modulates the gut microbiota and produces anti-cancer metabolites to protect against colorectal tumourigenesis. *Gut* 2021;71:2011–21.
16 Wilck N, Matus MG, Kearney SM, *et al*. Salt-responsive gut commensal modulates T(H)17 axis and disease. *Nature* 2017;551:585–9.
17 Cervantes-Barragan L, Chai JN, Tianero MD, *et al*. Lactobacillus Reuteri induces gut intraepithelial Cd4(+)Cd8$\mathbf{A}\alpha$(+) T cells. *Science* 2017;357:806–10.
18 Sato Y, Fu Y, Liu H, *et al*. Tumor-immune profiling of CT-26 and colon 26 syngeneic mouse models reveals mechanism of anti-PD-1 response. *BMC Cancer* 2021;21:1222.
19 Castle JC, Loewer M, Boegel S, *et al*. Immunomic, genomic and ranscriptomic characterization of CT26 colorectal carcinoma. *BMC Genomics* 2014;15:190.
20 Zelante T, Iannitti RG, Cunha C, *et al*. Tryptophan catabolites from microbiota engage aryl hydrocarbon receptor and balance mucosal reactivity via interleukin-22. *Immunity* 2013;39:372–85.
21 Gertsman I, Gangoiti JA, Nyhan WL, *et al*. Perturbations of tyrosine metabolism promote the indolepyruvate pathway via tryptophan in host and microbiome. *Mol Genet Metab* 2015;114:431–7.
22 Kim M, Tomek P. Tryptophan: a Rheostat of cancer immune escape mediated by immunosuppressive enzymes IDO1 and TDO. *Front Immunol* 2021;12:636081.
23 Jin U-H, Lee S-O, Sridharan G, *et al*. Microbiome-derived tryptophan metabolites and their aryl hydrocarbon receptor-dependent agonist and antagonist activities. *Mol Pharmacol* 2014;85:777–88.
24 Mezrich JD, Fechner JH, Zhang X, *et al*. An interaction between Kynurenine and the aryl hydrocarbon receptor can generate regulatory T cells. *J Immunol* 2010;185:3190–8.
25 Opitz CA, Litzenburger UM, Sahm F, *et al*. An endogenous tumour-promoting ligand of the human aryl hydrocarbon receptor. *Nature* 2011;478:197–203.
26 Siska PJ, Jiao J, Matos C, *et al*. Kynurenine induces T cell fat catabolism and has limited suppressive effects in vivo. *EBioMedicine* 2021;74:103734.
27 Rehman S-U, Saeed A, Saddique G, *et al*. Synthesis of sulfadiazinyl acyl/aryl Thiourea derivatives as calf intestinal alkaline phosphatase inhibitors, pharmacokinetic properties, lead optimization, lineweaver-burk plot evaluation and binding analysis. *Bioorg Med Chem* 2018;26:3707–15.
28 To KKW, Tomlinson B. Targeting the ABCG2-overexpressing multidrug resistant (MDR) cancer cells by PPARγ agonists. *Br J Pharmacol* 2013;170:1137–51.
29 Jenkins RW, Barbie DA, Flaherty KT. Mechanisms of resistance to immune checkpoint inhibitors. *Br J Cancer* 2018;118:9–16.
30 Zhuo Q, Yu B, Zhou J, *et al*. Lysates of lactobacillus acidophilus combined with CTLA-4-blocking antibodies enhance antitumor immunity in a mouse colon cancer model. *Sci Rep* 2019;9:20128.
31 Haduch A, Bromek E, Kuban W, *et al*. The engagement of cytochrome P450 enzymes in tryptophan metabolism. *Metabolites* 2023;13:629.
32 Gillam EM, Notley LM, Cai H, *et al*. Oxidation of Indole by cytochrome P450 enzymes. *Biochemistry* 2000;39:13817–24.
33 Tang K, Wu YH, Song Y, *et al*. Indoleamine 2,3-Dioxygenase 1 (Ido1) inhibitors in clinical trials for cancer immunotherapy. *J Hematol Oncol* 2021;14:68.
34 Desbonnet L, Garrett L, Clarke G, *et al*. The probiotic bifidobacteria Infantis: an assessment of potential antidepressant properties in the rat. *J Psychiatr Res* 2008;43:164–74.
35 Valladares R, Bojilova L, Potts AH, *et al*. Lactobacillus Johnsonii inhibits Indoleamine 2,3-Dioxygenase and alters tryptophan metabolite levels in biobreeding rats. *FASEB J* 2013;27:1711–20.
36 Zhai L, Dey M, Lauing KL, *et al*. The Kynurenine to tryptophan ratio as a prognostic tool for glioblastoma patients enrolling in immunotherapy. *J Clin Neurosci* 2015;22:1964–8.
37 Modoux M, Rolhion N, Mani S, *et al*. Tryptophan metabolism as a pharmacological target. *Trends Pharmacol Sci* 2021;42:60–73.
38 Laurans L, Venteclef N, Haddad Y, *et al*. Genetic deficiency of Indoleamine 2,3-Dioxygenase promotes gut microbiota-mediated metabolic health. *Nat Med* 2018;24:1113–20.
39 Gutiérrez-Vázquez C, Quintana FJ. Regulation of the immune response by the aryl hydrocarbon receptor. *Immunity* 2018;48:19–33.
40 Lamas B, Richard ML, Leducq V, *et al*. CARD9 impacts colitis by altering gut microbiota metabolism of tryptophan into aryl hydrocarbon receptor ligands. *Nat Med* 2016;22:598–605.
41 Goettel JA, Gandhi R, Kenison JE, *et al*. AHR activation is protective against colitis driven by T cells in humanized mice. *Cell Rep* 2016;17:1318–29.
42 Campesato LF, Budhu S, Tchaicha J, *et al*. Blockade of the AHR restricts a Treg-macrophage suppressive axis induced by L-Kynurenine. *Nat Commun* 2020;11:4011.
43 Hezaveh K, Shinde RS, Klötgen A, *et al*. Tryptophan-derived microbial metabolites activate the aryl hydrocarbon receptor in tumor-associated macrophages to suppress anti-tumor immunity. *Immunity* 2022;55:324–40.
44 Virk MS, Arttamangkul S, Birdsong WT, *et al*. Buprenorphine is a weak partial agonist that inhibits opioid receptor desensitization. *J Neurosci* 2009;29:7341–8.
45 Zhang XY, Soufi S, Dormuth C, *et al*. Time course for blood pressure lowering of beta-blockers with partial agonist activity. *Cochrane Database Syst Rev* 2020;9:CD010054.